Measurement of Articulation Angle by Image Template Matching

Journal Title
XX(X):1–14

DOI: 10.1177/ToBeAssigned
www.sagepub.com/
SAGE

Christopher de Saxe[1,2] and David Cebon[3]

Abstract

Articulated heavy goods vehicles and Long Combination Vehicles (LCVs) offer improved efficiency and emissions but reduced low-speed manoeuvrability and high-speed stability compared to rigid lorries. Active control systems can help to address these issues but require additional instrumentation, particularly articulation angle sensing. Existing commercial and research solutions for articulation sensing are limited either in terms of measurement accuracy or practicality. In this paper a camera-based articulation angle sensing concept using template-matching and an Unscented Kalman Filter is investigated, including detailed simulation and full-scale vehicle experiments. The effects of aliasing and trailer pitch angle are studied, and a correction model for trailer pitch is proposed. The sensing system demonstrates superior measurement accuracy compared to the published literature, with RMS errors of 0.8–1.8 degrees for articulation angles up to 37 degrees in full-scale experiments. The sensor solution proposed in this work addresses more of the practical criteria for this problem than the comparable solutions in the literature. It does so through the novel camera and image processing system which is unique to this application. The proposed sensor offers acceptable measurement accuracy in real-time, is non-contact, requires minimal knowledge of trailer parameters, and is compatible with semi-trailers and rigid draw-bar trailers.

Keywords

articulation angle, articulated vehicle, heavy goods vehicle, template-matching, computer vision, rotation measurement.

Introduction

Inland freight transport is critical to developed and developing economies, and the majority of this freight is moved by Heavy Goods Vehicles (HGVs). Improving the efficiency of HGVs has attracted commercial and research attention due to its impact on the cost of logistics, and more recently due to stringent CO_2 emissions targets. Methods for improving HGV efficiency vary in cost, practicality and barriers to introduction. For example, developments in IC engine technology are nearing saturation and provide gains of only 1–2% (1; 2). Low rolling resistance tyres and aerodynamic improvements are relatively low cost and offer better benefits (1–5% and 6-9%) (1; 2). Alternative fuels and hybrid/full electric powertrains present moderate to good efficiency benefits, but present significant cost, infrastructural and practical barriers to introduction at present.

In comparison, it is possible to achieve large gains of 11–19% (3) with relatively minor barriers to introduction by using larger vehicle combinations to carry more freight with fewer vehicles. Examples include the 'Longer Semi-Trailer' (LST) combination in the UK (4) and Long Combination Vehicles (LCVs) such as B-doubles and the 'Nordic Combination'. The effectiveness of these vehicles has been proved in implementations and trials in a number of countries including Australia, Sweden, UK and South Africa (5). Truck and trailer combinations with one or more articulation points tend to exhibit reduced low-speed manoeuvrability and high-speed stability. This can often be addressed through the use of active control technologies such as autonomous/assisted reversing (*e.g.* (6)), combined braking and steering control (*e.g.* (7)), and jacknife control (*e.g.* (8)). However, the additional instrumentation and

[1]Council for Scientific and Industrial Research, Pretoria, South Africa
[2]University of the Witwatersrand, Johannesburg, South Africa
[3]Department of Engineering, University of Cambridge, Cambridge, U.K.

Corresponding author:
Christopher de Saxe, CSIR Built Environment, P.O. Box 395, Pretoria 0001, South Africa.
Email: cdsaxe@csir.co.za

sensing required for these systems is often commercially impractical.

Importantly, these active systems all require articulation angle sensing between truck and trailer, or between subsequent trailers, as this is a critical indicator of articulated vehicle dynamic behaviour. Current commercial and research articulation sensors are either trailer-based, require significant modifications to the trailer, or have insufficient accuracy for control applications. In applications where control processing and actuation is tractor-based, it is desirable that articulation sensing should also be tractor-based, so that the system is wholly independent of the trailer.

In this work, a tractor-based articulation angle sensor concept is presented, which utilises a single camera, template-matching, and an Unscented Kalman Filter (UKF). The paper includes an overview of the template-matching method, and details of simulation and full-scale experiments conducted on a tractor semi-trailer combination. Performance was benchmarked against the state-of-the-art, and shown to offer improved measurement accuracy while also presenting practical benefits.

Related Work

Various articulation sensors exist either commercially or for research and development work. Examples include: a kingpin sensor commercially available from Vehicle Systems Engineering B.V. Netherlands (the 'VSE sensor') (9), a prototype magnetic sensor by AB electronic Ltd (the 'Orbisense' sensor) (10), and a custom string potentiometer solution (10). TRIDEC (Netherlands) use a custom articulation angle sensor as part of their active trailer steering system (11). These are all trailer-based sensors. The VSE and Orbisense sensors require significant modifications to the trailer kingpin and the string potentiometer requires a physical connection between tractor and semi-trailer. The Orbisense sensor was never commercialised, for reasons including insufficient resolution for active-trailer steering applications (10).

With the exception of the Orbisense^{TM} sensor, these sensors are examples of 'contact-type' sensors. For semi-trailers the fifth wheel is subjected to high static and dynamics loads and is a dirt and grease-prone environment, with potentially negative effects on the longevity of these sensors. For this application a good case can be made for a non-contact sensing solution.

State observer methods for estimating articulation angle of tractor semi-trailers for jackknife prevention have been proposed by Bouteldja *et al.* (12) and Chu *et al.* (13). Bouteldja *et al.* (12) adopted a state observer and an Extended Kalman Filter (EKF) and evaluated the system in simulation. Articulation angle results were not presented but comparable results for tractor yaw angle were given. Chu *et al.* (13) achieved good accuracy at small angles, but reduced accuracy at larger angles (20°) and under low friction conditions. Ehlgen *et al.* (14) adopted state estimation of articulation angle as part of a blind spot detection system, achieving moderate accuracy.

In other state estimation systems such as that of Cheng and Cebon (15), measurements from yaw rate sensors on both the tractor and trailer are often included as inputs to a Kalman Filter. The difference in these yaw rate measurements would provide a measurement of articulation rate, which could then be integrated to give the articulation angle. However, this solution assumes the availability of non-standard tractor and trailer-based yaw rate sensors on the vehicle, and would also introduce sensitivities to initial conditions and to integration drift.

The use of cameras for non-contact articulation angle measurement has been proposed by Schikora *et al.* (16), Caup *et al.* (17), Harris (18) and Fuchs (19; 20). For tractor semi-trailers, Schikora *et al.* (16) proposed using an encoder plate attached to the underside of the semi-trailer, viewed from a camera beneath. For draw-bar trailers they proposed placing infrared diodes on the front of the trailer, detected using an infrared camera on the back of the towing vehicle. The encoder plate system has a good claimed accuracy but performance of the infrared system is not clear.

Caup *et al.* (17) employed a rear-facing camera for draw-bar trailers, assuming the hitch location and draw-bar length to be known. They utilised a type of template-matching method, trained to optimise parameter sets, and an 'alpha-beta' filter. Moderate accuracy was demonstrated in vehicle tests.

Harris (18) also utilised a rear-facing camera for tractor semi-trailer combinations and investigated three image processing methods, assuming a planar (flat) trailer front surface. In the first method, homography decomposition was used to find the angle between observed images and a 'datum' image captured at zero articulation, achieving a frame rate of 0.2 fps. The second method utilised stereo vision, in which the generated point cloud was projected onto the horizontal plane and a RANSAC scheme was used to extract the rectangular trailer outline and infer its angle, yielding relatively large errors (up to 18°) and frame rate of 0.014 fps. It is possible that the algorithm could be refined to improve accuracy and frame rate.

Table 1. Summary of existing articulation angle estimation work

Ref.	Method	Validation	$\Gamma_{\max}$ (°)	$\epsilon_{\max}$ (°)
(12)	State observer	Sim.	90	8
(13)	State observer	Sim.	3–20	0.3–10
(14)	State observer	Veh.	48	5.4
(16)	Infrared vision	Veh.	-	-
(16)	Encoder	Veh.	90	0.3
(17)	Vision (templates)	Veh.	20–55	5.5–7.6
(18)	Vision (homog.)	Sim.	17–90	3.2–8.4
(18)	Vision (stereo)	Veh.	17–52	3.3–18
(19)	Vision (markers)	Sim.	50	0.5
(20)	Vision (markers)	Sim.	15–30	0.6

Harris briefly introduced a template-matching method, and a limited evaluation suggested the possibility of improved accuracy and computation speed compared to the first two methods. Only a single data point was considered to illustrate the concept using the CAD model, yielding a measurement error of 0.28°. Computation time per template comparison was 0.14 s, though multiple comparisons would be required per frame. The method is limited to planar trailers, and the underlying trailer model excludes translational trailer motion which could yield errors at higher articulation angles. This work was later expanded in (21) in which the concept was validated in small scale experiments, however computation was still comparably slow at 1 fps.

In 2014, Fuchs *et al.* (19) presented a camera-based articulation angle measurement concept for draw-bar trailers, using markers on the trailer and knowledge of vehicle geometry and camera location. The concept was tested in simulation. With perfect knowledge of camera location, a sub-1° accuracy was obtained, but errors rose significantly when uncertainty in camera location was incorporated. In (20), Fuchs *et al.* added a Kalman Filter to their system yielding improved accuracy.

Maximum measurement errors $\epsilon_{\max}$ were obtained from the above literature where possible, and are summarised in Table 1. Performance is categorised according to the maximum articulation angle assessed ($\Gamma_{\max}$) and the validation technique used (vehicle tests or simulation). In summary, there is a gap in the current state-of-the-art for a non-contact sensor which is accurate over a good range of articulation angle (validated in full-scale experiments), does not require modifications to or artificial markers on the trailer, and which assumes minimal knowledge of the trailer.

Summary of the Template-Matching Method

The visual template-matching concept for articulation angle sensing for HGVs is summarised in Figure 1 (21). The concept builds on preliminary work by Harris (18), using

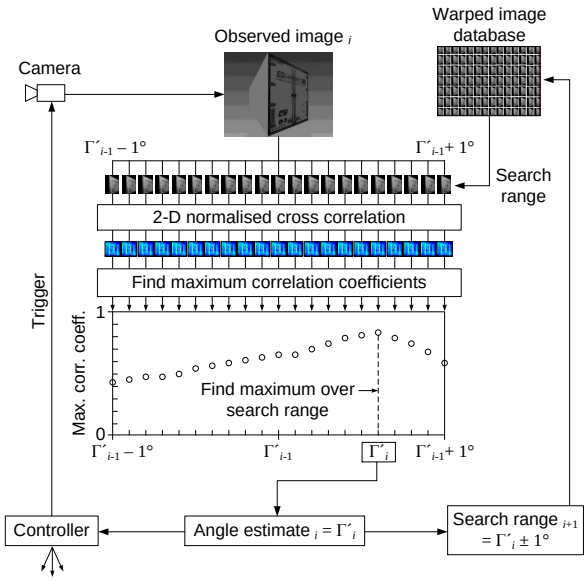

Figure 1. Template-matching method (21). Search range = ±1°, increment = 0.1°

a single camera mounted to the rear of the tractor and a template-matching image processing method to determine articulation angle Γ.

To initialise the algorithm, a single image of the front of the trailer is required, captured during a straight-line driving manoeuvre while the trailer is straight ($\Gamma \approx 0°$). This 'datum image' is 'warped' through increments of articulation angle to generate a database of images of how the front face of the trailer should appear at given articulation angles (a 'lookup table'). When presented with real-time 'observed' images from the camera, real-time articulation angle estimation is performed by comparing each observed image with images in the database and determining the best 'match'. An Unscented Kalman Filter (UKF) (22) is used to smooth the resulting measurements, using a simple kinematic vehicle model.

Assuming a planar trailer front, warping of the datum image can be achieved using a planar homography transformation. An image of the planar trailer face at $\Gamma \neq 0°$ is related to the datum image ($\Gamma = 0°$) through a planar homography P. Denoting homogeneous image coordinates as $\tilde{\mathbf{w}} = \xi[u, v, 1]^{\mathsf{T}}$, and the datum image as $\tilde{\mathbf{w}}_0$, the homography can be described by (23):

$$\tilde{\mathbf{w}} = \mathrm{P}\tilde{\mathbf{w}}_0 \tag{1}$$

$$\mathrm{P} = \mathrm{K}\left[\xi\left(\mathrm{R} + \frac{1}{d}\mathbf{T}\mathbf{N}^{\mathsf{T}}\right)\right]\mathrm{K}^{-1} \tag{2}$$

where K is the camera calibration matrix, ξ is an unknown scale parameter, R and $\mathbf{T}$ are the camera rotation and

translation between viewpoints, $\mathbf{N}$ is the normal to the observed plane at $\Gamma = 0°$, and d is the perpendicular distance to the plane at $\Gamma = 0°$.

Values of R, $\mathbf{T}$ and $\mathbf{N}$ for a tractor semi-trailer are:

$$\mathrm{R} = \begin{bmatrix} \cos\Gamma & 0 & \sin\Gamma \\ 0 & 1 & 0 \\ -\sin\Gamma & 0 & \cos\Gamma \end{bmatrix} \quad (3)$$

$$\mathbf{T} = \begin{bmatrix} (h+d)\sin\Gamma \\ 0 \\ (h+d)(1-\cos\Gamma) \end{bmatrix} \quad (4)$$

$$\mathbf{N} = \begin{bmatrix} 0 & 0 & 1 \end{bmatrix}^{\mathsf{T}} \quad (5)$$

where h is the trailer front overhang and d is the distance from the camera to the trailer face at $\Gamma = 0°$. Figure 2 shows an example datum trailer image being warped through $\Gamma = 37°$ by the homography P, for representative values of d and h.

Comparing real-time images against the warped images in the database is achieved using 'fast' normalised 2-dimensional cross correlation (NCC) (24). The maximum correlation coefficient over the NCC function is used as the similarity metric between images, with a higher correlation indicating a better match. The pixel location of the match defines the centre of a region of interest to search for the highest correlation coefficient in the next image frame. The range of Γ for database images compared (the 'search range') was limited to $\pm 1°$ from the previous estimates to minimise the number of image correlations computed.

From equations 2 and 4, the method assumes that knowledge of h and d are available. In addition, the UKF assumes knowledge of the hitch offset and trailer tractor and trailer wheelbases (see (25)). Hence, the concept is partly reliant on information about the trailer, but these parameters can be assumed to be typical values or could be estimated online. No physical alterations or connections to the trailer are required as distinct from alternative sensors.

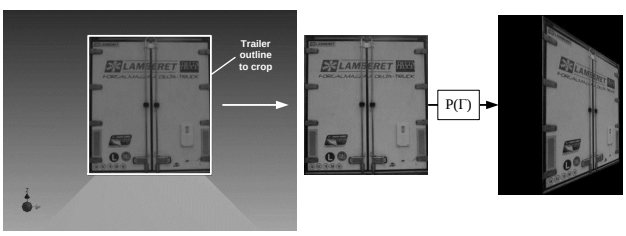

Figure 2. Warping the datum image through transformation P (Γ = 37°)

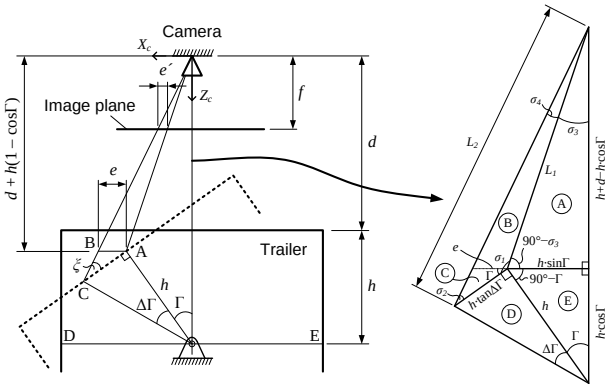

Figure 3. Incremental lateral motion behaviour of the trailer in the image plane

The overall algorithm is denoted 'TM+UKF' (template-matching + UKF). It was implemented in MATLAB (26) on a 64-bit Windows system with a 6-core 3.2GHz Core i7 processor. The VLFeat (27) and OpenCV (28) open source libraries were used for image warping and manipulation. The normxcorr2 MATLAB function, incorporating the method of Lewis (24), was used for image matching.

640×480 resolution greyscale images were used, but observed and template images were automatically cropped to exclude background image data. A database search range of $\pm 1°$ was used, and a tracking region of interest size of 60×40 pixels was used between frames. Distortion was corrected in real time using OpenCV functions.

The articulation angle increment between database images was 0.2°, resulting in 11 image comparisons to perform per frame. Database images were down-sampled by one pyramid level before calculating the NCC. These settings gave a framerate of 6–10 fps, compared to 0.65 fps for an equivalent implementation of Harris' concept (18) (0.14 s $\times$ 11 images). Variations in frame rate were due to the manner in which the template images were cropped according to articulation angle, resulting in smaller images at larger articulation angles.

Kinematic analysis

It is useful to study the relationship between trailer motion (Γ) and the resultant lateral pixel motion in the images (Δu). Consider Figure 3 which shows the trailer at angle Γ, and rotated by a small increment $\Delta\Gamma$ from this position. For the centre of the trailer face, the 'observed' lateral displacement is denoted e, where 'observed' means incorporating the perspective projection process, as if the imaging plane were located at the centre of the trailer face.

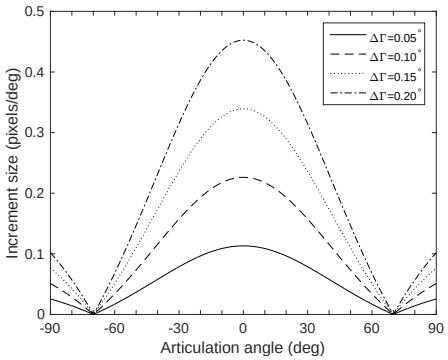

Figure 4. Incremental motion behaviour $|\Delta u|$ as a function of articulation angle Γ and increment size $\Delta\Gamma$ (VGA resolution, d = 2.3 m, h = 1.2 m)

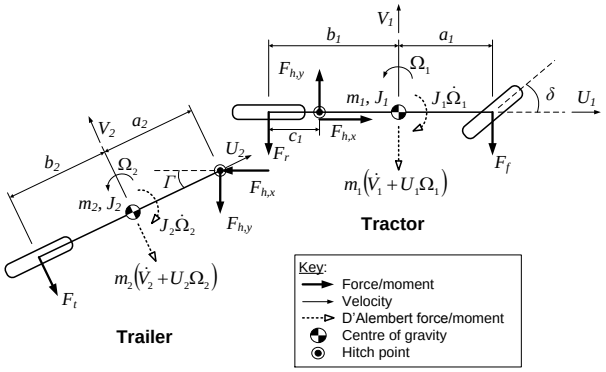

Figure 5. 3-degree-of-freedom vehicle model

Using the accompanying geometric detail in Figure 3, and assuming $\Delta\Gamma$ to be small, e may be calculated as follows:

$$e = -\frac{\Delta\Gamma h \cos(\Gamma + \sigma_4 + \sigma_3)}{\cos(\sigma_4 + \sigma_3)} \tag{6}$$

where

$$\sigma_4 = \sin^{-1}\ldots \left(\frac{\Delta\Gamma h \cos(\Gamma + \sigma_3)}{\sqrt{h^2\sin^2\Gamma + Z^2 - \Delta\Gamma h\cos\Gamma(2h^2\sin^2\Gamma + 2Z^2)}}\right) \tag{7}$$

$$\sigma_3 = \tan^{-1}\left(\frac{h\sin\Gamma}{Z}\right) \tag{8}$$

$$Z = d + h(1 - \cos\Gamma) \tag{9}$$

and where Z is the camera-reference co-ordinate of A. The lateral pixel motion Δu may then be calculated as follows:

$$\Delta u(\Gamma, \Delta\Gamma) = \left(\frac{f}{Z}\right) e \tag{10}$$

where f is the camera focal length.

The above equations may be used to examine the behaviour of Δu as Γ and $\Delta\Gamma$ are varied, where $\Delta\Gamma$ may be interpreted as the increment size of the warped image database (provided it is small). Figure 4 shows the variation in Δu with Γ and $\Delta\Gamma$ for $d = 2.3$ m, $h = 1.2$ m and a resolution of (640×480). This was generated for selected values of $\Delta\Gamma$ $(0.05°, 0.1°, 0.15°, 0.2°)$. The figure can be scaled linearly with variations in resolution, and will prove useful later when explaining the behaviour of measurement errors.

It is clear from the plots that $\Delta u = 0$ for a particular magnitude of Γ which is denoted $\Gamma_{\lim}$. This represents the point where the normal to the trailer face is perpendicular to the line of sight of the camera (see Figure 3). At this point, incremental movement of the trailer face is parallel to this ray and produces no lateral displacement in the image plane. Beyond this point the face is no longer visible. (Figure 4 shows the translation of the face in the opposite direction beyond this point, as the trailer continues to rotate.) From Figure 3, this is the point where $\sigma_2 = 0°$ and so $e = \Delta u = 0$. The value of Γ at this point is a function of h and d only and can be calculated according to:

$$\Gamma_{\lim} = \cos^{-1}\left(\frac{h}{h+d}\right) \tag{11}$$

Knowledge of this point is useful because it describes the limit beyond which the front face of the trailer can no longer be used for template-matching or other algorithms. For $h = 1.2$ m and $d = 2.3$ m, $\Gamma_{\lim} = 69.95°$.

Simulation Experiments

The simulation environment consisted of a tractor semi-trailer vehicle model and a CAD-based visual model. The vehicle model was used to generate appropriate articulation angle signals for a given steer input and vehicle speed. The visual model was used to generate representative image data to match these articulation angle signals.

Simulation Model

A dynamic 3 degree-of-freedom 'bicycle model' of a tractor semi-trailer was used to simulate vehicle motion, shown in Figure 5. Constant speed, linear tyres and negligible pitch and roll motion were assumed, and left and right tyres were reduced to a single tyre at the axle centre. Tyres are in reality highly non-linear beyond small slip angles, and exhibit complex transient behaviour (see for example (29; 30)). However, the linear tyre assumption was deemed adequate for this exercise given that only representative articulation angle signals were sought for validation. Although a representative sinusoidal articulation

signal may have sufficed, for example, a signal generated with an underlying vehicle model with simplified tyres offered increased realism to the simulation.

Equations of motion were derived using force balances, moment balances about the hitch point, and kinematic constraints at the hitch point. These can be summarised as follows:

$$m_1\left(\dot{V}_1 + U_1\Omega_1\right) + F_f\cos\delta + F_r - F_{h,y} = 0 \quad (12)$$

$$m_2\left(\dot{V}_2 + U_2\Omega_2\right) + F_t + F_{h,y}\cos\Gamma + F_{h,x}\sin\Gamma = 0 \quad (13)$$

$$(a_1+c_1)F_f\cos\delta + c_1 m_1(\dot{V}_1 + U_1\Omega_1) + \ldots \quad (14)$$
$$J_1\dot{\Omega}_1 - (b_1 - c_1)F_r = 0$$

$$(a_2+b_2)\,F_t + a_2 m_2\left(\dot{V}_2 + U_2\Omega_2\right) - J_2\dot{\Omega}_2 = 0 \quad (15)$$

$$\Omega_2 = \Omega_1 + \dot{\Gamma} \quad (16)$$

$$V_2 = (V_1 - (b_1 - c_1)\Omega_1)\cos\Gamma - U_1\sin\Gamma - a_2\Omega_2 \quad (17)$$

$$U_2 = U_1\cos\Gamma + (V_1 - (b_1 - c_1)\Omega_1)\sin\Gamma \quad (18)$$

$$F_f = C_f\alpha_f \qquad F_r = C_r\alpha_r \qquad F_t = C_t\alpha_t \quad (19)$$

$$\begin{aligned}\alpha_f &= \tan^{-1}\left[(V_1 + a_1\Omega_1)/U_1\right] - \delta\\ \alpha_r &= \tan^{-1}\left[(V_1 - b_1\Omega_1)/U_1\right]\\ \alpha_t &= \tan^{-1}\left[(V_2 - b_2\Omega_2)/U_2\right]\end{aligned} \quad (20)$$

Subscripts 1 and 2 denote the tractor and trailer units, and subscripts f, r and t denote the tractor front, tractor rear and trailer axles respectively. Variables m and J are vehicle mass and moment of inertia about the centre of gravity; a, b, c are lengths (see Figure 5); C is the tyre cornering stiffness; F is the lateral tyre force; $F_{h,x}$ and $F_{h,y}$ are longitudinal and lateral hitch forces; U and V are longitudinal and lateral velocities; Ω is yaw rate; Γ is the articulation angle; δ is the steer angle at the front axle; α is the tyre side-slip angle.

Equations 12 to 20 were solved in MATLAB (26) using a standard ordinary differential equation (ODE) solver. Dynamic vehicle parameters were taken from (18) for a Volvo tractor unit and box-type semi-trailer; and d and h were set to 2.3 m and 1.2 m as before. Full details of the simulation parameters may be found in (25).

A single degree-of-freedom CAD model of a tractor semi-trailer was created in Autodesk Inventor (31) to produce image data to accompany measurements of Γ from the vehicle model, shown in Figure 6. Visual characteristics of the trailer were taken from photographs of an existing research vehicle combination. A virtual camera was located behind the tractor cab. This functioned as a simple 'pin-hole' camera with no distortion. Camera intrinsic parameters

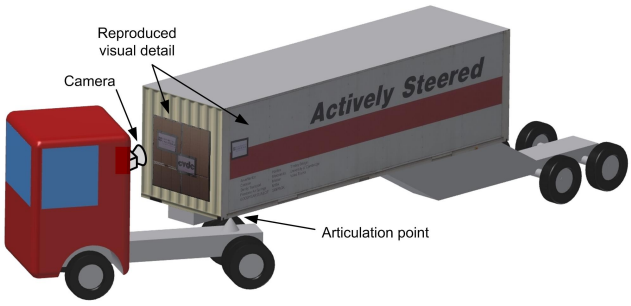

Figure 6. 1 degree-of-freedom CAD simulation model

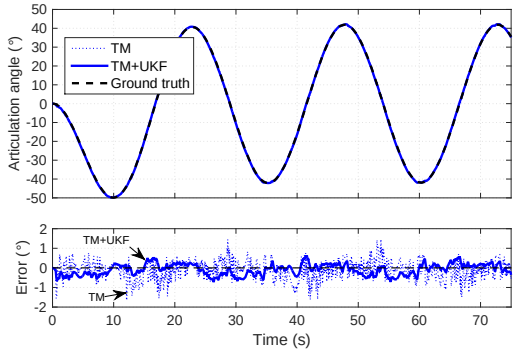

Figure 7. Simulation results, $\Gamma \leq 50°$. Template-matching includes $1\times$ down-sampling and $0.2°$ search increment

(K) were calculated using simple relationships for a pin-hole camera according to image resolution and field-of-view.

Simulation Results

A sinusoidal steer angle signal was input to the vehicle model to generate an articulation angle response, and associated image data were generated from the CAD model. Speed was kept constant at 6 km/h. The steer input was used as the input for the UKF, with added noise of standard deviation $0.1°$. For the UKF, the standard deviations of the measurement and process noise were set to $0.48°$ and $0.06°$ respectively.

Figure 7 shows an example time history and error signal generated by the simulation. Template-matching measurements with and without the UKF (TM dashed line, TM+UKF solid line) are shown for comparison. RMS and maximum errors were $0.30°$ and $0.73°$ respectively ($0.49°$ and $1.65°$ without the UKF).

Figure 8 shows the *unfiltered* TM errors as a function of articulation angle. A number of 'striations' are evident (clearest for $-\Gamma$), with a vertical spacing of approximately $1°$. These striations are due to aliasing as limited by image resolution. The errors are not symmetric about $\Gamma = 0°$: this is attributed to a small misalignment of the camera in the CAD model (it was not possible to align it perfectly with a specified coordinate axis).

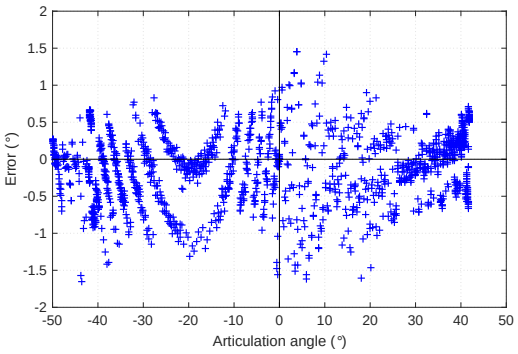

Figure 8. Simulation errors, $\Gamma \leq 50°$. Template-matching includes $1\times$ down-sampling and $0.2°$ search increment

To study the effects of aliasing in more detail, the simulation was performed again at full resolution (no down-sampling) with a search increment of $0.1°$. Individual data points were analysed for indications of aliasing which could be attributed to image resolution.

Figures 9a and 9b show the variations of correlation coefficient with articulation angle within the search range for selected low-Γ and high-Γ data points respectively. Well defined peaks and troughs are clear: a result of aliasing due to the fixed pixel-width sampling size. At $\Gamma \approx 3.5°$ (Figure 9a) the spacing between peaks is approximately 5 increments, or $0.5°$. At $\Gamma \approx 41.5°$ (Figure 9b) the spacing is approximately 9 increments, or $0.9°$. Both these results agree with the incremental motion behaviour exhibited in Figure 4 for the $0.1°$ increment size.

Figures 9c and 9d show a comparison between a good result (small error) and a bad result (larger error). An accurate measurement occurs when the true value of Γ lies near a peak, and poor measurements occur when Γ lies in a trough. In addition, when the true value of Γ lies near a trough, the two peaks either side of it are often similar in magnitude, resulting in large 'jumps' in error (equal to the peak spacing in magnitude) as the estimate jumps from one peak to the other on sequential time steps. This is demonstrated by viewing two sequential data points in Figure 9e and f. This sharp jump in error from $-0.5°$ to $+0.25°$ is clear, and was repeated cyclically at the same value of Γ. This effect can be seen to be the cause of the striations in Figure 8.

In the absence of any external disturbances therefore, the magnitude of errors exhibited are constrained to the magnitude of the aliasing effect, which in turn is a function of the system geometry and image resolution according to Figure 4. For the current geometry the maximum peak spacing is $0.45°$ which correlates well with the observed noise in the error signal (a standard deviation of $0.48°$).

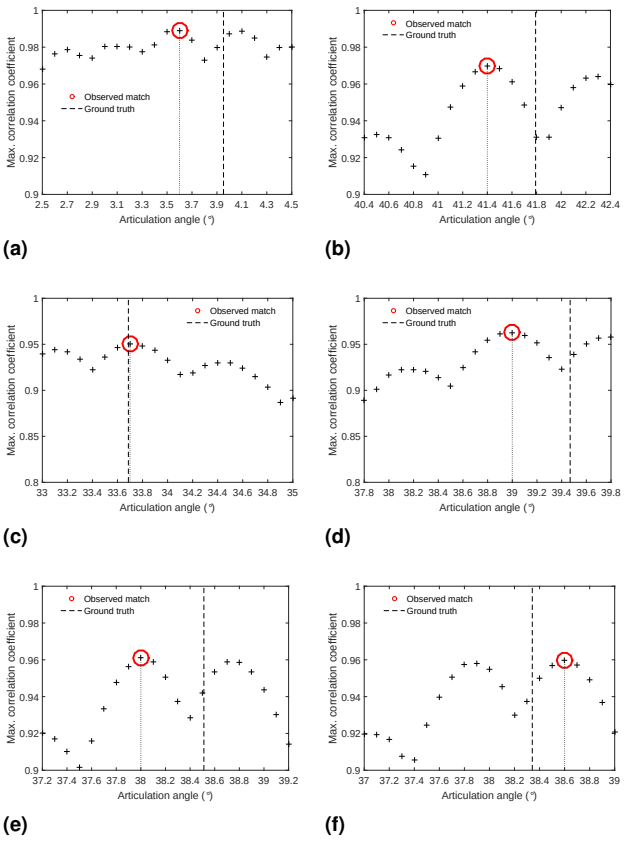

Figure 9. Aliasing effects: (a) small Γ, (b) large Γ, (c) good match, (d) bad match, (e) before jump (t_i), (f) after jump (t_{i+1})

Full-Scale Vehicle Experiments

Vehicle and instrumentation

Vehicle testing was carried out on an articulated vehicle combination consisting of a 4×2 tractor unit and a tri-axle, box-type semi-trailer, shown in Figure 10a. Parameters d and h were measured to be 886 mm and 1575 mm respectively ($\Gamma_{\text{lim}} = 68.9°$). A Point Grey Flea3 USB 3.0 camera was fitted to a bracket behind the tractor cabin, facing the front of the semi-trailer (Figure 10b). A 2.8–8 mm lens was used, with the focal length set near 2.8 mm to give a wide field of view. A flat surface was attached to the otherwise corrugated front of the trailer. To account for the loss in visual detail, arbitrary artificial visual texture was added on top of this (Figure 10c). A VSE articulation angle sensor was used to obtain 'ground truth' measurements (9) (Figure 10d). Images were captured in greyscale at 640×480 and at 20 fps.

A schematic of the vehicle instrumentation is given in Figure 11. Tractor speed and steer angle measurements for the UKF were acquired via a speed sensor on the drive axle and a string potentiometer on the steer axle. Analogue sensor signals were digitised and logged on both tractor and trailer.

Images were logged using a Linux computer in the tractor cab controlled by a Python script. Image trigger signals and

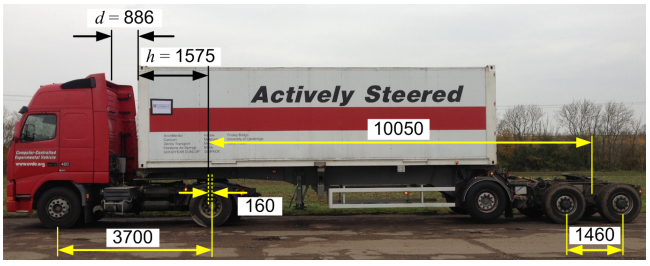

(a)

(b)

(c)

(d)

Figure 10. Test vehicle and instrumentation: (a) test vehicle (dimensions in mm), (b) camera behind the cab, (c) visual texture on trailer front, (d) VSE articulation angle sensor viewed from the top of the kingpin assembly

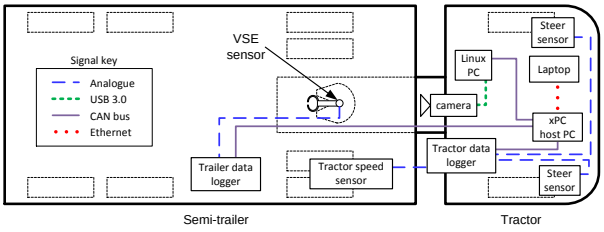

Figure 11. Vehicle instrumentation layout

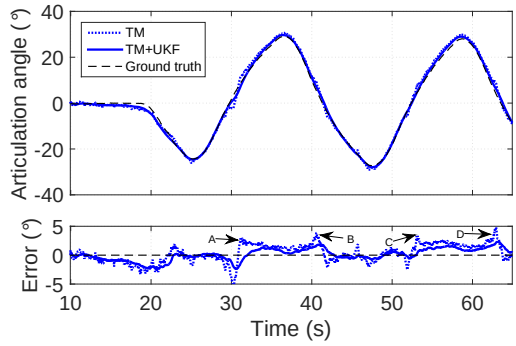

(a)

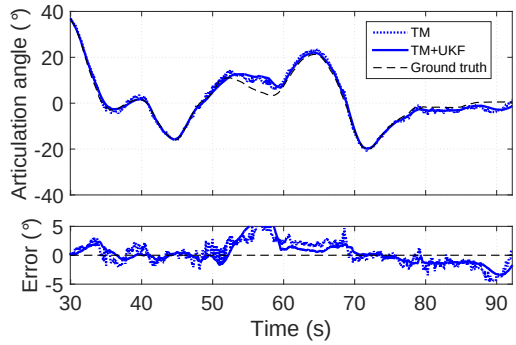

(b)

Figure 12. Vehicle test time histories, planar trailer: (a) per30 B, (b) gen A

sensor signals were synchronised via a host PC running SIMULINK xPC Target. A personal laptop computer was used as the xPC 'host' computer for data logging and general test control.

Testing was carried out on flat tarmac at Bourn airfield near Cambridge. Two types of manoeuvre were carried out: a periodic step steer input with articulation angles up to 30° (denoted 'per30') and a 'general' driving manoeuvre (a pseudo-random set of turns) (denoted 'gen'). Three runs of each manoeuvre were conducted.

Vehicle speed was approximately constant at 5 km/h for the step steer tests and variable in the range 0–10 km/h for the general driving tests. Steering input was manual in both cases, though controlled to an approximately repeatable steer amplitude and frequency in the step steer tests.

The camera was calibrated using the 'Camera Calibration Toolbox for MATLAB' (32), and real-time distortion correction was incorporated into the Python script. A datum image was collected once during a single straight line driving manoeuvre, and was used for all six tests. For the UKF, measurement noise covariance W was determined experimentally to be $(1.45°)^2$. The process noise covariance, Q, was tuned to $(0.06°)^2$ through trial and error on initial datasets.

Results

Typical results for a periodic and general driving manoeuvre are given in Figure 12a and 12b respectively. Unfiltered template-matching results ('TM') and template-matching results with the UKF ('TM+UKF') are shown. Error signals (relative to the VSE sensor) are given beneath each plot. In general, the TM+UKF measurements compare well with the ground truth, with errors rarely exceeding 2°. Errors are larger than were observed in the idealised CAD simulations as expected. Errors up to approximately ±0.5° can be attributed to aliasing as observed in the CAD simulations, in accordance with Figure 4. Remaining errors must therefore be attributable to external factors, such as transient short-wavelength pitch and roll motions of the trailer due to the rough road, or steady-state deviations from the underlying yaw-plane articulation model.

Recurring systematic errors are evident which are clearest in the periodic steer tests (Figure 12a). These are indicated by the regions A to B and from C to D (shown on error signal). These errors are also evident in Figure 12b at 53–60 s, but are less obvious because articulation angle variations are not

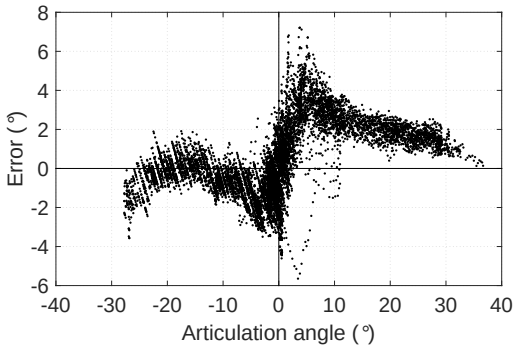

Figure 13. Errors vs. articulation angle, planar trailer, all tests overlaid

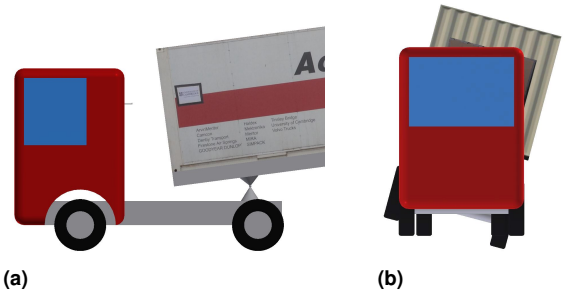

Figure 14. Added pitch (a) and roll (b) degrees of freedom to CAD model

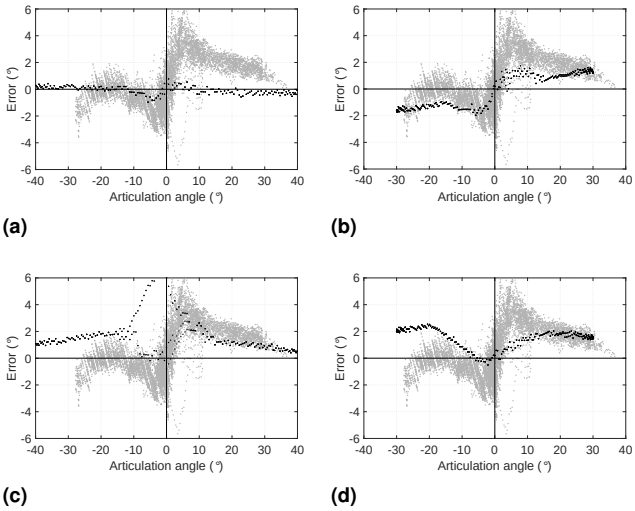

Figure 15. Errors vs. articulation angle for the six CAD variations. Vehicle test results are shown in grey for comparison: (a) Original, (b) 2° trailer pitch, (c) 2° trailer roll, (d) 2° camera yaw

periodic in these tests. These errors could not be correlated with observed transient variations in roll and pitch motion in the image sequences.

The recurring error behaviour is clear when examining variations of error with articulation angle, as shown in Figure 13. Results from all six tests have been overlaid. The systematic error trends are clear, and are consistent for both periodic and general driving manoeuvres. The trend can be viewed as having two components: an over-arching 'smooth' approximately linear component varying from approximately $-2°$ at $\Gamma = -30°$ to $+2°$ at $\Gamma = +30°$, and a zero-crossing component in the region $-15°$ to $+10°$. The zero-crossing component yields peaks in errors at approximately $\pm 5°$.

From comparison with the simulation results (Figure 8), aliasing appears to have given rise to the noise component over the whole articulation range, but cannot explain the smooth and zero-crossing error trends. The underlying yaw plane model made a number of assumptions about the relative camera-trailer motion which included assumptions that: relative motion is constrained to the yaw plane, the camera was mounted perfectly with its optical axis perpendicular to the trailer front face, the magnitudes of d and h are known accurately, and that the datum image was obtained at exactly zero articulation angle and perpendicular to the camera optical axis. The most likely cause of deviations from these assumptions include camera misalignment or a steady state pitch, roll or yaw of the trailer caused by suspension and hitch characteristics. Steady state pitch, roll and yaw offsets from either camera misalignment or trailer pose would alter the values of d and h from their assumed nominal values and would alter the assumption that $\mathbf{N} = [0, 0, 1]^\top$ for the datum image.

Error Analysis and Correction Model

To investigate the effects of offset pitch, roll and yaw rotations in a controlled environment, the CAD model was updated to match the dimensions of the test vehicle and to incorporate pitch and roll degrees-of-freedom (see Figure 14). The combined vehicle and CAD model was used to generate test sequences as before, but with steady-state pitch, roll and yaw angles imposed on the trailer. The resultant error trends as a function of articulation angle were then compared to the vehicle test results. Simulations were conducted for a range of pitch, roll and yaw offsets.

Selected results are given in Figure 15, where they have been overlaid on the field-testing results for comparison. Figure 15a shows the nominal case with no pitch, roll or yaw offsets. Figure 15b, c and d show the effects of adding $2°$ pitch, roll and yaw offsets respectively. The addition of pitch reproduces both the smooth and zero-crossing errors trends for both $+\Gamma$ and $-\Gamma$, while roll and yaw offsets only reproduce the trend for limited ranges of Γ.

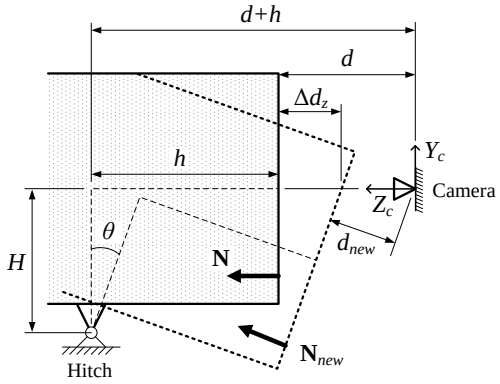

Figure 16. The effect of trailer pitch angle on parameters d and **N** (side view)

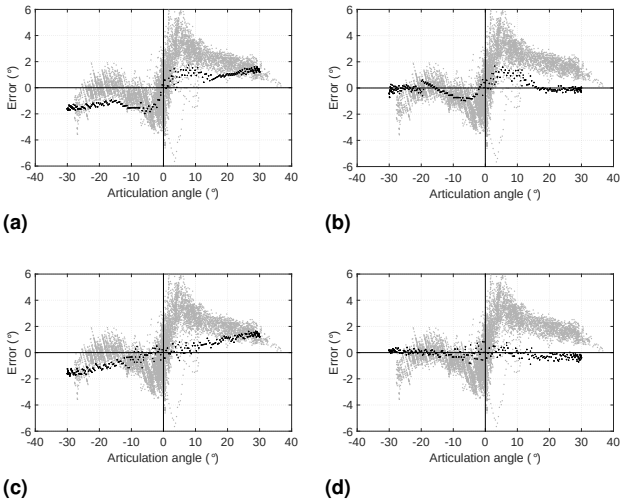

Figure 17. Correction results for the 2° trailer pitch CAD scenario. Vehicle test results shown in grey: (a) uncorrected, (b) $-2°$ of pitch correction, (c) edge detection, (d) $-2°$ pitch correction and edge detection

In order to correct for the effect of a pitch offset, a pitch correction model was developed as an extension to the original yaw-plane model. The proposed correction model is illustrated in Figure 16, showing a simplified side view of the trailer-camera system. Assuming articulation to still occur in a plane aligned with the trailer yaw plane (*i.e.* h is unchanged), only parameters d and **N** are affected.

For a pitch angle of θ, d would be corrected to d_{new} as indicated in the diagram. The component of the change in d in the z-direction (along the optical axis), Δd_z, and the resultant corrected value of d, d_{new}, may be derived by geometry and shown to be:

$$\Delta d_z = [H\sin\theta - h(1-\cos\theta)] + \ldots \\ \tan\theta\,[h\sin\theta + H(1-\cos\theta)] \quad (21)$$

$$d_{\text{new}} = (d - \Delta d_z)\cos\theta \quad (22)$$

where H is the height of the optical axis above the pitch centre, assumed to be at the kingpin. For the test vehicle H was measured to be 1750 mm.

Accompanying this would be a change in **N** to reflect the non-zero pitch angle of the datum plane. This can be incorporated by pre-multiplying the nominal value of **N** by the pitch component of a rotation matrix as follows:

$$\mathbf{N}_{\text{new}} = \begin{bmatrix} 1 & 0 & 0 \\ 0 & \cos\theta & -\sin\theta \\ 0 & \sin\theta & \cos\theta \end{bmatrix} \begin{bmatrix} 0 \\ 0 \\ 1 \end{bmatrix} = \begin{bmatrix} 0 \\ -\sin\theta \\ \cos\theta \end{bmatrix} \quad (23)$$

The effectiveness of the pitch correction was assessed by implementing it in the CAD simulation and investigating various values of θ. Uncorrected and corrected simulation results for $\theta = 2°$ are shown in Figures 17a and 17b respectively. It is clear that the smooth error component has been corrected, but that the zero-crossing trend at small Γ has been largely unaffected.

As part of an investigation into the cause of this, edge detection was added as a pre-processing step before NCC was carried out. Results for the 2° pitch case with no pitch correction but with edge detection are shown in Figure 17c. Interestingly, this has resulted in an almost complete correction of the zero-crossing component of the error trend. Results with both pitch correction and edge detection are shown in Figure 17d, showing an almost perfect reproduction of the baseline CAD case shown in Figure 15a. This suggests that the zero-crossing error trend component could be related to the underlying nature of the NCC step.

However, upon reprocessing the vehicle test results, the addition of edge detection was shown to severely reduce the robustness of the system. After the first small transient pitch or roll disturbance the measurements would become unstable, giving rise to unbounded errors. Edge detection was therefore not carried forwards. It is possible that the zero-crossing trend could also be a result of bidirectional roll motion which changes at the transition from $-\Gamma$ to $+\Gamma$, possibly a result of lash in the fifth wheel for example.

The field testing measurements were reprocessed with the pitch correction model. The effect of a range of pitch angles was assessed, and a value of $\theta = 2.2°$ yielded the most improvement in the smooth error component. Errors versus Γ are shown in Figure 18 with and without pitch correction. The steady trend from $\epsilon = -2°$ to $+2°$ has been eliminated and the peak errors around $\Gamma = \pm 5°$ have been reduced slightly.

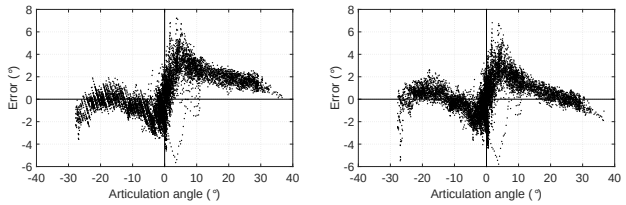

Figure 18. The effect of pitch correction on the error trends of vehicle tests: (a) no correction, (b) 2.2° pitch correction

Table 2. Results summary: full-scale vehicle tests

		Original		Corrected	
	$\Gamma_{\max}$ (°)	$\epsilon_{\max}$ (°)	ϵ_{RMS} (°)	$\epsilon_{\max}$ (°)	ϵ_{RMS} (°)
per30 A	31	4.21	1.40	3.69	1.04
per30 B	29	2.37	1.04	2.42	0.86
per30 C	29	3.39	1.14	2.70	0.75
gen A	37	7.24	2.04	6.75	1.79
gen B	33	3.67	1.32	2.83	1.02
gen C	23	2.63	0.97	2.30	0.88
Ave. of tests		3.92	1.32	3.45	1.06

A summary of maximum and RMS errors is given in Table 2. The pitch correction reduced the average maximum error and average RMS error by $0.47°$ and $0.26°$ respectively in the TM+UKF results, yielding an average maximum error of $3.45°$ and an average RMS error of $1.06°$.

Performance benchmark

A comparison of the final pitch-corrected results with the published state-of-the-art is shown in Figure 19. Maximum errors observed in individual vehicle tests are shown as a function of maximum articulation angle tested. (RMS errors would make a more insightful comparison, but these were not available in all the literature.) Results from Schikora (16) have been omitted: the encoder system requires substantial trailer modifications, and accuracy information for the diode system is not available. It is clear that the TM+UKF algorithm exhibits improved accuracy compared to the literature. The articulation range assessed is smaller than the other concepts, but the system was demonstrated up to $50°$ in simulation and should be functional up to $\Gamma_{\text{lim}} = 68.9°$ for the test vehicle considered.

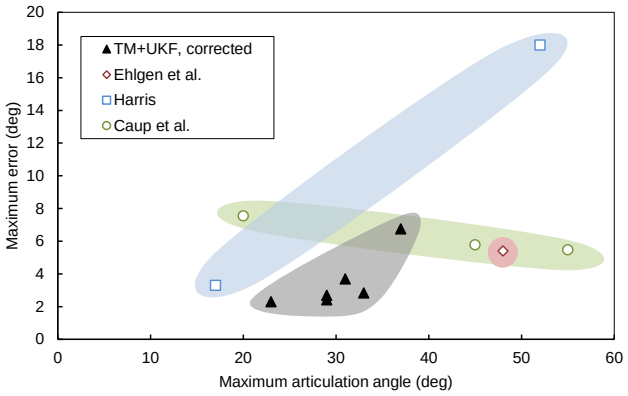

Figure 19. Performance benchmark against published vehicle test data

Conclusions and Future Work

A non-contact tractor-based articulation angle sensor for articulated vehicles was presented to address shortcomings of existing commercial and research-stage sensors. The concept was validated in detailed simulations and full-scale vehicle experiments. The limiting effects of aliasing were highlighted in simulation, and corroborated in full-scale vehicle tests. The sensitivity of measurement errors to articulation angle was investigated, highlighting trailer pitch angle as a primary cause. The model equations were updated to correct for trailer pitch, and the correction was shown to effectively reduce errors in the full-scale vehicle tests. Errors of 0.8–1.8° RMS were obtained for articulation angles of up to 37°.

Future work in the short term will explore more efficient image comparison metrics, automated pitch angle detection, and sensitivity to varying lighting and weather conditions. The remaining errors not attributable to pitch angle will be investigated to further improve measurement accuracy. These may be attributable to roll angle or camera alignment and so these effects will be studied in more detail. In the medium term, feature tracking algorithms will be explored for full 3-dimensional trailer pose estimation, potentially negating the effects of trailer pitch and roll, and removing the need for knowledge of trailer dimensions. Applicability to other truck and trailer combinations will also be investigated.

This work helps to improve the commercial viability of the next generation of articulated vehicle control systems. In turn, such systems ultimately improve the viability of long combination vehicles which have demonstrated benefits for logistics efficiency and carbon emissions. Control systems such as autonomous reversing, combined braking and steering control and jackknife control rely heavily on articulation angle sensing, but existing solutions have had limited commercial feasibility. The system proposed in this work addresses many of the limitations of these existing solutions, specifically accuracy, dependence on multiple known vehicle parameters, dependence on other sensors, and limited compatibility with different vehicle configurations.

Declaration of conflicting interests

The author(s) declared no potential conflicts of interest with respect to the research, authorship, and/or publication of this article.

Funding

This work was funded by the Cambridge Commonwealth, European and International Trust (CCEIT), the Council for Scientific and Industrial Research (CSIR, South Africa), and the Cambridge Vehicle Dynamics Consortium (CVDC). At the time of writing the Consortium consisted of the University of Cambridge with the following partners from the heavy vehicle industry: Anthony Best Dynamics, Camcon, Denby Transport, Firestone Industrial Products, Goodyear, Haldex, MIRA, SDC Trailers, Tinsley Bridge, Tridec, Volvo Trucks, and Wincanton.

References

[1] Baker H, Cornwell R, Koehler E et al. Review of low carbon technologies for Heavy Goods Vehicles - Annex 1. Technical Report June, Department for Transport, London, 2009.

[2] Kay D and Hill N. Opportunities to overcome the barriers to uptake of low emission technologies for each commercial vehicle duty cycle. Technical report, The Low Carbon Vehicle Partnership, London, 2012. URL http://www.ricardo-aea.com/cms/overcoming-the-barriers-to-uptake-of-low-emission-technologies-for-heavy-goods-vehicles/?stage=Live.

[3] Leach DZ and Savage CJ. Impact assessment : High Capacity Vehicles. Technical report, University of Huddersfield, Huddersfield, 2012.

[4] DfT. Domestic road freight statistics, United Kingdom, 2015. Technical Report August, Department for Transport, London, 2016.

[5] OECD. Moving freight with better trucks. Technical report, International Transport Forum/OECD, Paris, 2011. DOI:10.1787/9789282102961-en. URL http://dx.doi.org/10.1787/9789282102961-en.

[6] Rimmer AJ and Cebon D. Implementation of reversing control on a doubly articulated vehicle. *J Dyn Syst Meas Control* 2017; 139(6): 061011–061011–9. URL http://dx.doi.org/10.1115/1.4035456.

[7] Morrison G and Cebon D. Combined emergency braking and turning of articulated heavy vehicles. *Vehicle System Dynamics* 2017; 55(5): 725–749. DOI:10.1080/00423114.2016.1278077. URL http://dx.doi.org/10.1080/00423114.2016.1278077.

[8] Chen LK and Shieh YA. Jackknife prevention for articulated vehicles using model reference adaptive control. *Proc Inst Mech Eng Part D J Automob Eng* 2011; 225(1): 28–42. DOI:10.1243/09544070JAUTO1513. URL http://dx.doi.org/10.1243/09544070JAUTO1513.

[9] VSE. Product information for ETS trailer, 2009. URL http://www.v-s-e.com/uploads/documents/leaflet-ets-trailer-en.pdf.

[10] Jujnovich BA. *Active steering of articulated vehicles*. Phd thesis, University of Cambridge, 2005.

[11] Tridec. Product overview: mechanical and hydraulic steering systems and axle suspensions, 2014. URL http://jic.jost-world.com/static/upload/pdf/FLY/32004_FLY_TRIDEC_Uebersicht_Image_160824_EN_SCREEN.pdf.

[12] Bouteldja M, Koita A, Dolcemascolo V et al. Prediction and detection of jackknifing problems for tractor semi-trailer. In *IEEE Veh. Power Propuls. Conf.* Windsor: IEEE. ISBN 1-4244-0158-5, pp. 1–6. DOI:10.1109/VPPC.2006.364272. URL http://ieeexplore.ieee.org/lpdocs/epic03/wrapper.htm?arnumber=4211300.

[13] Chu L, Fang Y, Shang M et al. Estimation of articulation angle for tractor semi-trailer based on state observer. In *Int. Conf. Meas. Technol. Mechatronics Autom.*, volume 2. Changsha City: IEEE. ISBN 978-1-4244-5001-5, pp. 158–163. DOI:10.1109/ICMTMA.2010.342. URL http://ieeexplore.ieee.org/lpdocs/epic03/wrapper.htm?arnumber=5459910.

[14] Ehlgen T, Pajdla T and Ammon D. Eliminating blind spots for assisted driving. *IEEE Transactions on Intelligent Transportation Systems* 2008; 9(4): 657–665. DOI:10.1109/TITS.2008.2006815. URL http://ieeexplore.ieee.org/lpdocs/epic03/wrapper.htm?arnumber=4674602.

[15] Cheng C and Cebon D. Parameter and state estimation for articulated heavy vehicles. *Vehicle System Dynamics* 2011; 49(1-2): 399–418. DOI:10.1080/00423110903406656. URL https://doi.org/10.1080/00423110903406656.

[16] Schikora J, Berg U and Zöbel D. Berührungslose Winkelbestimmung zwischen Zugfahrzeug und Anhänger. In Halang W and Holleczek P (eds.) *Aktuelle Anwendungen Tech. und Wirtschaft*. Informatik aktuell, Springer Berlin Heidelberg. ISBN 978-3-540-85323-7, 2009. pp. 11–20. DOI:10.1007/978-3-540-85324-4_2. URL http://dx.doi.org/10.1007/978-3-540-85324-4_2.

[17] Caup L, Salmen J, Muharemovic I et al. Video-based trailer detection and articulation estimation. In *IEEE Intell.*

Veh. Symp. Gold Coast: IEEE. ISBN 978-1-4673-2755-8, pp. 1179–1184. DOI:10.1109/IVS.2013.6629626. URL http://ieeexplore.ieee.org/lpdocs/epic03/wrapper.htm?arnumber=6629626.

[18] Harris MP. *Application of computer vision systems to heavy goods vehicles: visual sensing of articulation angle*. Mphil thesis, University of Cambridge, 2013.

[19] Fuchs C, Eggert S, Knopp B et al. Pose detection in truck and trailer combinations for advanced driver assistance systems. In *Proc. IEEE Intell. Veh. Symp.* Dearborn, MI: IEEE. ISBN 978-1-4799-3638-0, pp. 1175–1180. DOI:10.1109/IVS.2014.6856547. URL http://ieeexplore.ieee.org/lpdocs/epic03/wrapper.htm?arnumber=6856547.

[20] Fuchs C, Neuhaus F and Paulus D. Advanced 3-D trailer pose estimation for articulated vehicles. In *IEEE Intell. Veh. Symp.* Seoul: IEEE. ISBN 9781467372657, pp. 211–216.

[21] de Saxe CC and Cebon D. A visual template-matching method for articulation angle measurement. In *Proc. 18th IEEE Int. Conf. Intell. Transp. Syst.* Las Palmas: IEEE. ISBN 978-1-4673-6595-6, pp. 626–631. DOI:10.1109/ITSC.2015.108.

[22] Julier S and Uhlmann J. Unscented filtering and nonlinear estimation. *Proc IEEE* 2004; 92(3): 401–422. DOI:10.1109/JPROC.2003.823141. URL http://ieeexplore.ieee.org/lpdocs/epic03/wrapper.htm?arnumber=1271397.

[23] Ma Y, Soatto S, Kosecka J et al. Reconstruction from two calibrated views. In Antman SS, Marsden JE, Sirovich L et al. (eds.) *An Invit. to 3-D Vis. from images to Geom. Model.*, 1 ed, chapter 5. New York: Springer Science+Business Media. ISBN 978-0-387-00893-6, 2004. pp. 109–170.

[24] Lewis JP. Fast normalized cross-correlation. *Vis Interface* 1995; 10(1).

[25] de Saxe CC. *Vision-based trailer pose estimation for articulated vehicles*. Phd thesis, University of Cambridge, 2017.

[26] Mathworks. MATLAB R2013b, 2013. URL http://www.mathworks.co.uk/products/matlab/.

[27] Vedaldi A and Fulkerson B. VLFeat: An open and portable library of computer vision algorithms, 2008. URL http://www.vlfeat.org/.

[28] Bradski G. The OpenCV library, 2000. URL http://opencv.org/.

[29] Gipser M. FTire the tire simulation model for all applications related to vehicle dynamics. *Vehicle System Dynamics* 2007; 45(sup1): 139–151. DOI:10.1080/00423110801899960. URL https://doi.org/10.1080/00423110801899960.

[30] Mavros G, Rahnejat H and King P. Analysis of the transient handling properties of a tyre, based on the coupling of a flexible carcass-belt model with a separate tread incorporating transient viscoelastic frictional properties. *Vehicle System Dynamics* 2005; 43(sup1): 199–208. DOI:10.1080/00423110500140658. URL https://doi.org/10.1080/00423110500140658.

[31] NA. Inventor Professional 2013, 2013. URL http://www.autodesk.com/products/inventor/overview.

[32] Bouguet JY. Camera calibration toolbox for Matlab, 2004. URL http://www.vision.caltech.edu/bouguetj/calib_doc/index.html#ref.

Appendix

Notation

$a_{1,2}$	Distance from CoG to steer axle, hitch point
$b_{1,2}$	Distance from CoG to rear axle (tractor, trailer)
c	Hitch offset ahead of rear axle
$C_{f,r,t}$	Tyre cornering stiffness (front, rear, trailer)
d	Perpendicular distance from camera to trailer face at $\Gamma = 0°$
d_{new}	Pitch-corrected value of d
d_z	Component of d along the camera optical axis
e	'Observed' lateral displacement of the centre of the trailer face
f	Camera focal length
$F_{f,r,t}$	Lateral tyre force (front, rear, trailer)
$F_{h,x}$	Hitch force, longitudinal component
$F_{h,y}$	Hitch force, lateral component
h	Trailer front overhang
H	Optical axis height above the trailer pitch centre
$J_{1,2}$	Yaw moment of inertia about CoG (tractor, trailer)
K	Camera calibration matrix
$m_{1,2}$	Vehicle mass (tractor, trailer)
N	Normal vector of trailer face at $\Gamma = 0°$
$\mathbf{N}_{\text{new}}$	Pitch-corrected value of **N**
P	Planar homography matrix
Q	Process noise covariation
R	Camera rotation matrix
T	Camera translation vector
u	Horizontal image coordinate
$U_{1,2}$	Longitudinal velocity (tractor, trailer)
v	Vertical image coordinate
$V_{1,2}$	Lateral velocity (tractor, trailer)
$\tilde{\mathbf{w}}$	Image in homogeneous coordinates
$\tilde{\mathbf{w}_0}$	Datum image in homogeneous coordinates
W	Measurement noise covariance
Z	Camera-reference co-ordinate along the optical axis
$\alpha_{f,r,t}$	Tyre side-slip angle (front, rear, trailer)
Γ	Articulation angle
Γ_{lim}	Articulation angle beyond which the trailer face is not visible to the camera
Γ_{max}	Maximum articulation angle assessed
δ	Steer angle at front axle
ϵ_{max}	Maximum measurement error
ϵ_{RMS}	RMS measurement error
θ	Trailer pitch angle
ξ	Homogeneous scale parameter
$\sigma_{1,2,3,4}$	Various angles in the trailer rotation process
$\Omega_{1,2}$	Yaw rate (tractor, trailer)

Abbreviations

CAD	Computer-Aided Design/Drawing
CoG	Centre of Gravity
EKF	Extended Kalman Filter
HGV	Heavy Goods Vehicle
IC	Internal Combustion
LCV	Long Combination Vehicle
LST	Longer Semi-Trailer
NCC	Normalised Cross Correlation
ODE	Ordinary Differential Equation
RANSAC	Random Sample Consensus
RMS	Root Mean Square
TM	Template-Matching
UKF	Unscented Kalman Filter